Hindawi
Scientific Programming
Volume 2022, Article ID 9675526, 11 pages
https://doi.org/10.1155/2022/9675526

Research Article

A Novel Effective Edge-Based Image Denoising Algorithm

Anil Kumar Puli,[1] **K. Sateesh Kumar**,[2] **J. Brahmaiah Naik**,[3] **P. Janardhan Saikumar**,[4] **and Biruk Ambachew Adugna**[5]

[1]*Department of Electronics and Communication Engineering, CVR College of Engineering, Hyderabad, India*
[2]*Department of Electronics and Computer Engineering, Sreenidhi Institute of Science and Technology, Hyderabad, India*
[3]*Department of Electronics and Communication Engineering, Kallam Haranathareddy Institute of Technology, Guntur, India*
[4]*Department of Electronics and Communication Engineering, Audisankara Institute of Technology, Gudur, India*
[5]*Department of Computer Science, Ambo University, Ambo, Ethiopia*

Correspondence should be addressed to Anil Kumar Puli; anilkumar417@cvr.ac.in, K. Sateesh Kumar; sateeshk@sreenidhi.edu.in, and Biruk Ambachew Adugna; biruk.ambachew@ambou.edu.et

Received 25 April 2022; Revised 22 June 2022; Accepted 28 June 2022; Published 19 July 2022

Academic Editor: Punit Gupta

This article proposes an edge-based denoising algorithm to restore the original image, which is highly degraded by the salt and pepper noise. Most of the existing image denoising algorithms consider edge as a noise. Here, the proposed algorithm can set out to resolve this ambiguity. The concept of directional filters is being used to delineate the edges from noise. The proposed algorithm performance is tested for different noise densities ranging from 5% to 90% on both the greyscale and colour images. It is compared with the current state of art techniques using several performance metrics such as peak signal-to-noise ratio (PSNR), structural similarity index measure (SSIM) values, and image enhancement factor (IEF). The results showed that the proposed algorithm has achieved an improvement of 60% over the state of art techniques.

1. Introduction

Noise is produced in the image during the process of acquisition or added to the image during the transmission of the image over the wired or wireless medium. Nowadays, wireless channels are preferred compared to the wired channels [1]. The wireless medium is more prone to noise, and this may lead to image degradation which affects the image quality. There is a wide variety of noise which affects the quality of the image such as Gaussian noise, impulse noise, speckle noise, and random noise [2]. Impulse noise is also called as salt and pepper noise that arises due to the short presence of "on" and "off" of the pixel values due to surface degradation of the camera. The present article deals with the denoising salt and pepper noise from the noisy images. Unlike the other noise models, it does not add or multiply the original pixel values instead it replaces the pixel values either with 0 or 255 [3, 4]. It appears in the image due to the malfunctioning of the devices which capture the images. The salt and pepper noise comes under high-frequency content in the image. However, the edges in the image also come under the high-frequency content of the image [5]. So, there is a challenge in distinguishing the salt and pepper noise from this edge. In the literature, few works exist to delineate the edge from noise [6].

In the medical field, image denoising is very useful for accurate diagnosis, otherwise life may be destroyed. Traditional methods such as low-rank methods and sparse coding depend on the self-similarity of the image pixel values to denoise the noisy image [7]. The major problem with these traditional methods is that they remove or smooth the edge (fine detail) information in the image. The edge details in the image are similar to the noise which is equivalent to the high frequency.

The rest of the article is organized as follows: Section 2 presents the proposed noise detection algorithm. Section 3 deals with the proposed denoising algorithm. The experimental results and comparisons with the existing methods in terms of metrics such as PSNR, SSIM, and IEF are elaborated

in Section 4. Finally, the summary of the article is presented in Section 5.

2. Literature Review

The main aim of the image denoising is to minimize the amount of noise present in the image by retaining the original information in the image such as edges. The image denoising algorithms should not alter the edge information, texture information in the image should be preserved, and new artifacts should not be generated while denoising the image. The image denoising methods are broadly classified into two broad categories, namely spatial domain methods and transform domain methods. In the spatial domain method, the image is convolved with the low-pass filter mask/kernel for the removal of noise information from the image. The accuracy of the method depends on the weightage provided to the mask location in the image [8]. Spatial filtering is further divided into linear and nonlinear filters. Linear filters such as mean filter and Gaussian filter remove the noise content as well as the edge information from the image. These filters are suitable for the removal of Gaussian noise in the image. The nonlinear filters such as the median filter, weighted median filter, and bilateral filter remove the noise from the edge by retaining the edge information. These filters are useful in the removal of salt and pepper noise from the images. In general, the spatial filter removes the noise from the images at the expense of losing the edge information from the image [9].

Median filter is a nonlinear filter which is specifically designed for the removal of the salt and pepper noise from the image. The masks used in median filter are usually odd in size such as 3×3, 5×5, etc. The values within the mask are sorted, and the processing element is replaced with the middle values of the sorted element array. The computational complexity of the median filter is very low. But it fails to denoise the images, when the size of the image is small, or the variance of the noise level increases. The lower size of the mask is effective when the noise level in the image is low; and for the higher level of noise variance, the higher size mask is preferred. The adaptive median filter adjusts the size of the mask based on the level of noise variance [10].

Also, a wide variety of nonlinear spatial filters have been proposed to restore the original image, which is corrupted with noise. Among the various techniques, median filter (MF) has been widely used in the literature for the removal of salt and pepper noise. But the use of MF was effective when the noise density is very low, and it failed to recover the original image when the noise density is high [11]. There exists a relationship between the noise density and the size of the mask, which says that the size of the mask should be the minimum for a low noise density and vice versa. To improve the quality of the restored image in terms of PSNR, the size of the mask should be increased with the increase in noise density. Based on MF theory, adaptive median filter (AMF) was proposed by adjusting the size of the window based on noise variance ($\sigma 2$) in the image. However, the major drawback of the AMF is that it fails to preserve the edge information for a high noise density model [12]. Inspired by the AMF works, switching median filter (SMF) was proposed by adjusting the size of the mask with respect to the local threshold value. However, the value of the threshold varies dynamically, and it also depends on the number of noise pixels present in the vicinity of the current processing pixel [13]. The aforementioned filter-based method does not consider the local features; as a result, the edge information is not retained properly.

To deal with the edge information, a decision-based algorithm (DBA) with a 3×3 mask was proposed. This method simply replaces the noisy pixels based on the threshold value alone, which results in a streaking effect in the restored image [14]. To resolve the streaking effect, decision-based unsymmetric trimmed median filter (DBUTMF) was proposed. However, the method fails to denoise the image for a high value of noise variance (more than, 50%) [15]. A noise adaptive fuzzy switching median (NAFSM) algorithm was proposed. This method uses two stages to retrieve the original image from the noisy image [16]. In the first phase, the corrupted pixels of the noisy image are identified with the histogram. In the second phase, a suitable membership function is designed to filter these noisy pixels, and the value is modified based on the neighbourhood of the processing pixels [17]. Even though the technique is efficient, it has high time complexity. The other proposed method is the interquartile range (IQR) filter [18]. It is a nonlinear spatial filter that aims at removing the noise by preserving the edge information. The IQR process simply replaces the processing pixel with the mean of the surrounding non-noisy pixels [19]. All these methods are again valid for low-range noise variance image but not for high noise level. To tackle mild or high noise levels, adaptive IQR (AIQR) [20] filter was proposed; this varies the size of the mask with the noise density. It provides higher PSNR compared to the other methods, but it fails to preserve the edge information.

The transform domain methods transform the image from spatial domain to the frequency domain, and a suitable filter was applied to remove the noise and it is transformed to the spatial domain for a better visualization of the image [21]. But the frequency domain methods consume more processing time during conversion from the spatial domain to the frequency domain and vice versa [22]. The transform adaptive filtering is further classified into two categories, namely data adaptive and non-data adaptive [23].

In the data adaptive transform methods, principal component analysis (PCA) and independent component analysis (ICA) are employed as transform tools for the conversion process [24]. These methods assume that the noise is a high-frequency component and is present in the last band of the image frame. Among these two methods, ICA proves to be effective in the removal of the Gaussian noise from the images. But these methods suffer from the huge computational cost since it employs the sliding window algorithm [22]. These methods prove to be effective for the denoising of satellite images.

The non-data adaptive transform methods are classified into wavelet domain-based methods and spatial domain-based methods. The wavelet-based non-data adaptive

method decomposes the original image into sub-bands. These methods have been proved that it can remove the noise from the image and preserve the characteristics of the image. The performance of these wavelet methods relies on the selection of the basis function used in the denoising process. There are numerous basis functions available in the wavelet transform, and each basis function is designed for a specific application. Improper selection of the basis function leads to poor denoising performance [23].

Block-matching three-dimensional (BM3D) is a transform method which employs the 2-stage nonlocal collaborative filtering operation. The similar patches in the original image are stacked into 3-dimensional groups, and these groups are transformed using the wavelet domain methods. Then it is subjected to denoising by using the hard-thresholding algorithm [24]. By using inverse wavelet transforms and aligning the patches correctly, the denoised image is reconstructed [25]. This method proves to be effective when the noise variance is low and the performance degrades as the noise level in the image increases and hence artifacts are introduced into the denoised image [26].

The gradient-based image model uses the heavy-tailed distribution of the image gradient compared to the traditional-based models because they use the statistical model to predict the gradients of the image [27]. The gradient-based model suffers from the huge computational cost which incurs due to the estimation of the statistical parameters of the image dynamically during the runtime [28]. The deep learning methods achieve better accuracy compared to the statistical models and gradient-based models [29]. The deep learning models suffer from the problem that it requires a huge database for training and testing to improve the accuracy of the model [30]. One more problem with the deep learning models is the number of layers needed to denoise the image and the type of model required for denoising [31].

Bnou et al. proposed a machine learning-based model for image denoising. They used an unsupervised learning model in their work and proved that it presents better performance compared to the supervised learning model of image denoising [32]. They have modified the algorithm based on the dictionary-based model to improve the quality of performance [33]. The quality of the performance depends on the training samples [34]. When the number of images used for training increases, performance improves, but too much training degrades performance [35].

Patanavijit et al. proposed in his work a novel method for denoising the random-valued impulse noise. In the present work, the author has overcome the limitation of the adaptive median filter by a novel filter under both unsystematic intensity impulse and salt [36] and pepper noise [37].

Yan xing et al. proposed in their work about the usage of deep learning methods for the removal of salt and pepper noise from the images. A multilayer convolution neural network had been used in their work which consists of a convolution layer for extracting the useful features from the image, a max pooling layer for reducing the dimensionality of the image, and the activation function. But the proposed method requires a huge dataset for training and testing purposes [38]. The accuracy of the method depends on the training. Another drawback of this model is that every image has to be resized to fixed dimension of 224×224 or 124×124. The method requires a huge amount of time for training purpose also [39].

Limshuebchuey and Saejia compared various deep learning algorithms for the removal of noise from the images. They have compared the traditional methods with the deep learning models in terms of PSNR and SSIM. Deep learning clearly shows an upper hand compared to the traditional methods. But the major problem with the deep learning models is the time required for training and number of images required for training. The architecture of the model varies as the noise variance varies in the image. Gaussian noise and impulse noise had been used in their work for denoising [40].

Singh et al. used the autoencoder model for the image denoising. In this work, the authors used the deep convolutional neural network-based model VGG16 with the custom dataset of bad weather outdoor images via transfer learning. The sequential model 1 and model 2 are evaluated to have a smooth image. The model architecture using DCNN is designed, and training of the model is obtained using transfer learning. A model using an autoencoder is designed. To decrease training time and perform better, RELU is used. In CNN, the number of epochs with increased performance was identified. The author had never mentioned in his work the advantage of the VGG16 model in the work. However, the performance of the model depends on the transfer learning model used in the work [41].

Wang et al. used an unsupervised learning model for denoising the image. They have designed a network based on the modified iterative soft threshold algorithm (ISTA), which omitted the soft threshold to alleviate uncertainties introduced by empirically selected thresholds. In this network, we set the dictionary and code as trainable parameters. A loss function with a smooth penalty was designed to ensure that the network training can be implemented in an unsupervised manner. They fused the result obtained from the block matching 3D algorithm and the unsupervised model, which improves the result further [42].

This article proposes an edge-preserving denoising algorithm, which can discriminate the noisy pixels from the edge pixels. So, the final retrieved image would be clear from the salt and pepper noise and it preserves the edge information. Since this method uses a two-level adaptive filter to retrieve the values based on the direction of the edge, it is efficient and has less time complexity. The proposed algorithm was tested on both the grey as well as colour images and it has shown a good PSNR, SSIM, and IEF over the exiting methods.

3. Proposed Method

This study aims at the minimization of the impact of impulse noise and had not considered any other type of noise. The masks designed in this work were based on the statistical properties of the impulse noise. In general, denoising methods are suffered with the similarity between an edge and noise whose intensity value is always high. Because of

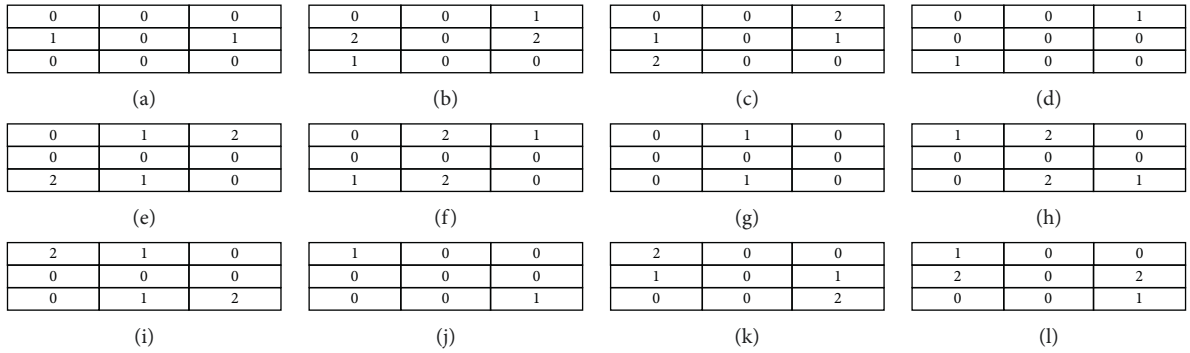

Figure 1: Edge-based kernels of order 3×3 for all possible edge directions in the image: (a) $0^\circ \leq \theta < 5^\circ$ and $175^\circ < \theta \leq 180^\circ$; (b) $5^\circ \leq \theta < 22.5^\circ$; (c) $22.5^\circ \leq \theta < 40^\circ$; (d) $40^\circ \leq \theta < 50^\circ$; (e) $50^\circ \leq \theta < 67.5^\circ$; (f) $67.5^\circ \leq \theta < 85^\circ$; (g) $85^\circ \leq \theta < 95^\circ$; (h) $95^\circ \leq \theta < 112.5^\circ$; (i) $112.5^\circ \leq \theta < 130^\circ$; (j) $130^\circ \leq \theta < 140^\circ$; (k) $140^\circ \leq \theta < 157.5^\circ$; and (l) $157.5^\circ \leq \theta < 175^\circ$.

this, edges are not perfectly discriminated from noise. This we achieved with the help of directional filters. Image denoising can be done either in the spatial domain or in the frequency domain. Frequency domain filtering needs the image to be transformed into the frequency domain from the spatial domain, then the suitable filter has to be applied for the removal of noise and then it has to be converted back into the spatial domain for the visualization purpose. Hence it requires a lot of computation for the process of denoising. In this study, spatial domain filtering is used since the computation time of the spatial domain filtering is less than that compared to the frequency domain filtering. The proposed method works only for the minimization of the impact of salt and pepper noise in the images [32]. The masks used in this study are specifically designed for the removal of salt and pepper noise by preserving the edges as discussed in the following section and are shown in Figure 1. The proposed algorithm is organized into three stages.

The first stage is to identify the noisy pixels based on the pixel values. While in the second stage, a combination of noisy and non-noisy pixel is approximated with a surrounding mean filter. Here, the size of the mask depends on the number of noisy pixels present in the neighbourhood of the current processing pixel. In the final stage, a special mask of fixed size 3×3 is applied to the processed noisy pixel in the direction of the noisy pixel(s); at this stage, edge and noisy pixels are distinguished.

In the first stage, a pixel is considered as noisy based on the threshold value, that is either minimum or maximum grey level value that is 0 or 255. This can be suggestible, because of the nature of salt and pepper noise. But all such values might not be considered as noise, some of the pixels are part of the image. In the second stage, adaptive IQR algorithm is utilized for denoising. This adaptive IQR algorithm works better than the existing median-based filters because of quartile values with soft thresholding.

This improves the performance of the denoising algorithm in various situations like high contrast and low contrast images. In the adaptive IQR filter, the initial size of the mask used is 3×3. If the number of uncorrupted pixels in the mask is less than the order of the mask, then the size of the mask is increased to a next higher order, that is 5,7,9 etc. In the third stage, the Sobel operator is used to find the direction of an edge at each one of the noisy processed pixels.

The processed noise pixel values are modified based on the direction of the edge information. The grey levels of the corrupted pixel values are updated based on the direction of the edges in the image of that window. Sobel operator consists of a pair of 3×3 convolution masks to obtain the spatial gradient of the image. These kernels are used to obtain the magnitude of the gradient component in the horizontal and vertical directions. The proposed edge denoising algorithm flowchart is shown in Figure 2.

This proposed algorithm is for greyscale images. To validate it for the colour images, repeat the steps from 2 to 6 on each one of the individually extracted R, G, and B channels. The edge orientation angle can be determined with the help of spatial gradient and is given below:

$$\boldsymbol{\theta} = \left(\frac{\mathbf{G_y}}{\mathbf{G_x}}\right). \tag{1}$$

3.1. Algorithm.

Step 1: Add the salt and pepper noise of known variance (5,10, . . ., 90) and zero-mean to the original image.

Step 2: Discriminate the noisy pixels from the non-noisy pixels in the image by using the hard-thresholding technique.

Step 3: As a preliminary process, denoise the image by applying the IQR algorithm.

Step 4: Delineate edge and noise using the spatial directional filters.

Step 5: Apply the edge-based mask for denoising the image.

Step 6: Evaluate the performance metrics such as PSNR, SSIM, and IEF for the denoised image with the original version.

Figure 3 depicts the Sobel mask for extracting horizontal and vertical edges using 3×3 mask. The left-hand side of the image is useful in extracting the vertical edges in the image. The right-hand side of image helps in extracting the horizontal

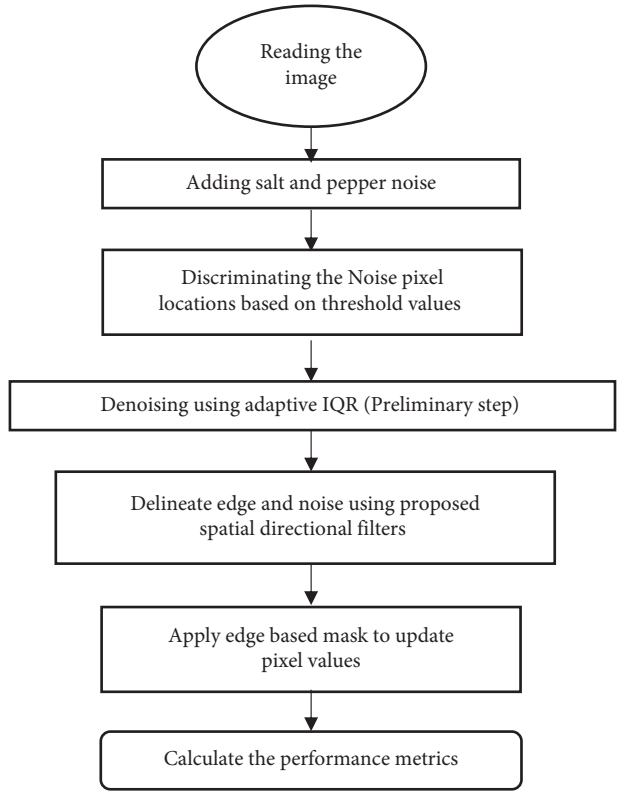

Figure 2: Flowchart of the edge-based denoising algorithm.

-1	0	+1
-2	0	+2
-1	0	+1

Gx

-1	-2	-1
0	0	0
+1	+2	+1

Gy

Figure 3: Sobel horizontal and vertical masks.

edges in the image. The strength of the edge and the direction of the edge information can obtained using these gradients.

Figure 1 shows that the range of direction of the edge in an image considered in this work is from 0° to 180°. This entire range is divided into 8 possible orientations (in degrees) such as 0, 22.5, 45, 67.5, 90, 112.5, 135, and 157.5. The 3×3 kernels are developed for each orientation and are represented in Figure 1(a)–1(l).

4. Results and Discussion

For this study, the image is subjected to a known amount of noise variance ranging from 5% to 90%. To demonstrate the efficacy of the proposed edge-based denoising (EBD) technique, the performance was compared with the existing denoising techniques such as median filter (MF), adaptive median filter (AMF), interquartile range filter (IQR), adaptive IQR (AIQR), based on pixel density filter (BPDF), and noise adaptive fuzzy switching median filter (NAFSM). The results are valid for both the greyscale and colour images. The performance metrics used for this study are PSNR, SSIM, and IEF. Mean squared error is defined as the cumulative of the squared error between the original image and the denoised output image and is shown in equation (2). The PSNR is commonly used as measure of quality reconstruction of image. It indicates the peak error in the image and is shown in (3). Structural similarity index is used to calculate the similarity between the images. This referential metrics considers image degradation which perceived changes in the form of structural information of the interdependence points and is shown in equation (4). μ defines the mean value of the image and σ defines the variance of the image. Image enhancement factor validates the enhanced factor of the images by comparing each and every pixel points which are modified after denoising [8]. It is calculated by taking the ratio between the sum of square of difference of original with the noise image and the sum of square of difference of denoised image with the noisy image and is shown in equation (5).

$$\mathrm{MSE} = \frac{1}{M * N}\left(\sum_{x=0}^{M-1}\sum_{y=0}^{N-1}\left(\mathrm{Orig}(x,y) - \mathrm{Output}(x,y)\right)^2\right), \tag{2}$$

$$\mathrm{PSNR} = 10 * \log_{10}\frac{255}{\mathrm{MSE}^{0.5}}, \tag{3}$$

$$\mathrm{SSIM} = \frac{\left(2 * \mu_x\mu_y + C1\right)\left(2 * \sigma_{xy} + C2\right)}{\left(\mu_x^2 + \mu_y^2 + C1\right)\left(\sigma_x^2 + \sigma_y^2 + C2\right)}, \tag{4}$$

(a) (b) (c) (d) (e)

(f) (g) (h)

Figure 4: Results of the proposed and standard methods when the image is corrupted with 30% noise density: (a) Original image with 30% noise density; (b) MF [8]; (c) AMF [9]; (d) IQR [15]; (e) AIQR [16]; (f) BPDF [28]; (g) NAFSM; and [13] (h) EBD.

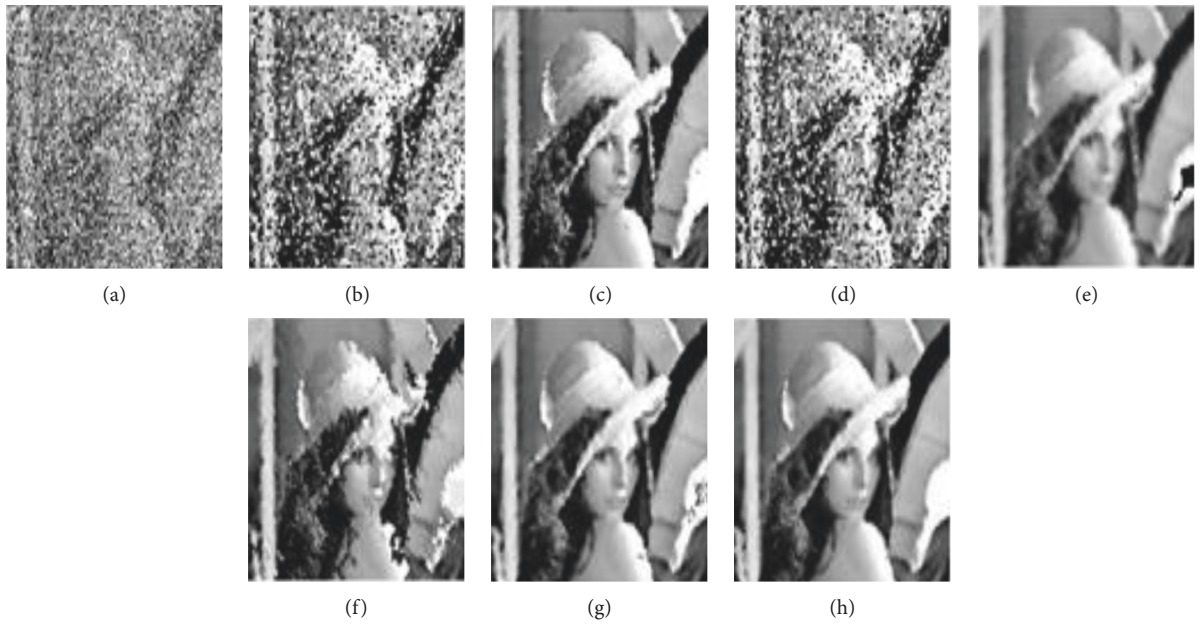

(a) (b) (c) (d) (e)

(f) (g) (h)

Figure 5: Results of the proposed and standard methods when the image is corrupted with 70% noise density: (a) Image with noise density of 70%; (b) MF [8]; (c) AMF [9]; (d) IQR [15]; (e) AIQR [16]; (f) BPDF [18]; (g) NAFSM [13]; and (h) EBD.

Table 1: Comparison of PSNR of different denoising algorithms (grey level).

Noise level (%)	MF [8]	AMF [9]	NAFSM [13]	IQR [16]	PSMF [27]	BPDF [28]	EBM
5	25.915	17.268	26.618	21.433	27.314	**31.323**	31.074
10	25.063	17.244	25.621	21.012	26.240	28.860	**29.848**
20	22.745	17.184	24.093	20.644	23.923	25.929	**27.795**
30	20.015	17.173	22.969	19.868	22.128	23.696	**26.070**
40	16.568	17.014	22.126	18.857	19.720	21.627	**24.346**
50	13.663	16.850	20.974	18.128	17.197	20.394	**22.990**
60	11.055	16.639	20.352	17.756	11.030	17.736	**21.191**
70	9.0188	16.291	19.110	17.226	8.995	15.452	**20.530**
80	7.1701	14.119	18.059	16.819	7.154	11.884	**19.153**
90	5.7660	10.320	15.925	15.817	5.757	8.229	**16.717**

Table 2: Comparison of SSIM of different denoising algorithms (grey level).

Noise level (%)	MF	AMF	NAFSM	IQR	PSMF	BPDF	EBM
5	0.895	0.612	0.954	0.919	0.953	0.979	**0.971**
10	0.882	0.610	0.939	0.910	0.936	0.965	**0.964**
20	0.828	0.608	0.904	0.884	0.893	0.934	**0.947**
30	0.715	0.605	0.875	0.846	0.836	0.896	**0.925**
40	0.514	0.595	0.844	0.786	0.742	0.842	**0.897**
50	0.331	0.585	0.809	0.727	0.600	0.785	**0.861**
60	0.195	0.568	0.772	0.679	0.203	0.686	**0.815**
70	0.117	0.545	0.725	0.638	0.121	0.570	**0.771**
80	0.058	0.413	0.656	0.593	0.060	0.350	**0.696**
90	0.029	0.196	0.526	0.532	0.029	0.184	**0.583**

Table 3: Comparison of IEF of different denoising algorithms (grey level).

Noise level (%)	MF	AMF	NAFSM	IQR	PSMF	BPDF	EBM
5	6.670	0.910	7.844	2.376	9.206	23.171	**21.883**
10	11.149	1.841	12.677	4.386	14.620	26.724	**33.551**
20	13.142	3.651	17.925	8.100	17.234	27.355	**42.039**
30	10.443	5.427	20.613	10.093	16.986	24.373	**42.100**
40	6.305	6.988	22.672	10.681	13.029	20.211	**37.803**
50	4.036	8.407	21.730	11.283	9.106	19.012	**34.560**
60	2.679	9.691	22.784	12.533	2.663	12.476	**27.642**
70	1.930	10.302	19.717	12.777	1.920	8.493	**27.343**
80	1.448	7.174	17.770	13.357	1.442	4.287	**22.866**
90	1.178	3.363	12.226	11.924	1.176	2.078	**14.670**

$$IEF = \frac{\sum_{i=0}^{M-1}\sum_{j=0}^{N-1}(\text{Noise}(i,j) - \text{Orig}(i,j))^2}{\sum_{i=0}^{M-1}\sum_{j=0}^{N-1}(\text{Output}(i,j) - \text{Orig}(i,j))^2}. \quad (5)$$

The qualitative analysis of comparison of the proposed method with other standard methods subjected to a noise variances of 30% and 70%, respectively, is shown in Figures 4 and 5 for the Lena image (greyscale). It is found that the performance metrics of the proposed method surpasses the other methods as the noise density increases. The quantitative analyses of all these results are tabulated in Tables 1–3. It has been observed that the proposed method outperforms when the noise density is greater than 10%. However, it is found that the proposed method shows a slightly less performance than the BPDF method when the noise variance is 5%.

As shown in Table 1, the PSNR metric obtained from various denoising techniques clearly reveals that EBM techniques outperforms the other techniques for various noise levels ranging from 5% to 90%. Similarly, the other metrics like SSIM and IEF are also inferred from Tables 2 and 3, respectively.

Figure 6 represents the comparison of PSNR metric on colour Lena image. It is observed that the proposed denoising technique produces a high-quality image even when the noise levels are high. Similar tabular representations are shown in Tables 4–6. In order to get a crisp overview, the pixel-level comparison is shown in Figure 7. Figure 6 shows the graphical representation of the PSNR metric obtained from various denoising techniques on greyscale Lena image. From Figure 6, it is clear that EBM techniques outperforms the other techniques for various noise levels ranging from 5% to 90%. Similarly, the other metrics like SSIM and IEF are also shown in Figures 7 and 8, respectively.

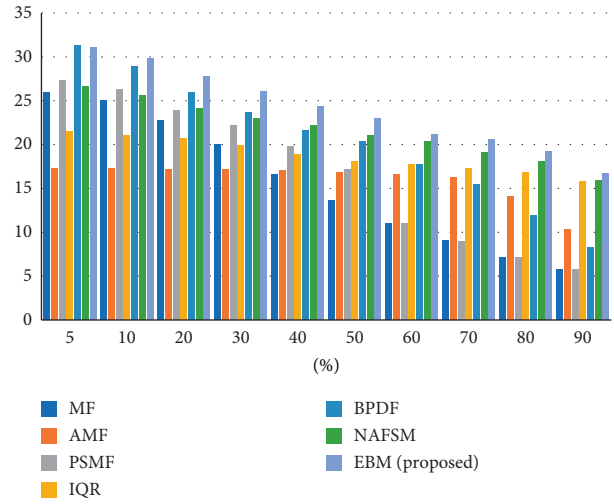

Figure 6: Graphical representation of comparison of PSNR for different denoising techniques.

Table 4: Comparison of PSNR for different algorithms (colour).

Noise level (%)	MF	AMF	NAFSM	IQR	PSMF	BPDF	EBM
5	31.995	24.202	40.932	35.895	36.873	41.128	**44.203**
10	31.309	24.139	38.061	35.511	34.325	38.035	**41.200**
20	27.760	24.034	34.980	34.442	30.457	34.686	**37.961**
30	23.131	23.935	32.988	32.931	27.508	32.287	**35.621**
40	18.629	23.817	31.630	31.181	24.374	30.373	**33.803**
50	14.977	23.649	30.375	29.350	18.050	28.392	**31.935**
60	12.067	23.409	29.285	28.112	12.002	26.340	**30.307**
70	12.064	23.403	29.330	28.138	11.998	26.361	**30.413**
80	7.874	18.965	26.698	26.500	7.843	19.640	**26.985**
90	6.357	12.240	23.178	**25.229**	6.343	12.026	**23.982**

Table 5: Comparison of SSIM for different algorithms (colour).

Noise level (%)	MF	AMF	NAFSM	IQR	PSMF	BPDF	EBM
5	0.983	0.940	0.998	0.993	0.995	0.998	**0.999**
10	0.981	0.938	0.996	0.992	0.991	0.996	**0.998**
20	0.963	0.936	0.992	0.991	0.981	0.992	**0.995**
30	0.908	0.935	0.988	0.987	0.966	0.987	**0.992**
40	0.781	0.933	0.983	0.982	0.935	0.980	**0.989**
50	0.602	0.930	0.978	0.974	0.762	0.971	**0.984**
60	0.412	0.926	0.973	0.966	0.421	0.957	**0.978**
70	0.412	0.925	0.973	0.966	0.422	0.957	**0.978**
80	0.140	0.823	0.954	0.952	0.148	0.876	**0.958**
90	0.058	0.471	0.908	0.939	0.062	0.658	**0.934**

Table 6: Comparison of IEF for different algorithms (colour).

Noise level (%)	MF	AMF	NAFSM	IQR	PSMF	BPDF	EBM
5	24.244	4.030	189.809	59.516	74.546	198.571	**403.122**
10	41.014	7.869	194.167	107.928	82.145	192.982	**400.035**
20	36.354	15.418	191.704	169.333	67.655	179.135	**380.822**
30	18.834	22.663	182.235	179.890	51.596	155.088	**334.146**
40	8.867	29.282	176.943	159.596	33.285	132.479	**291.884**
50	4.789	35.276	165.995	131.105	9.7193	105.140	**237.722**
60	2.938	39.998	156.569	118.998	2.894	79.0375	**200.898**
70	2.938	39.998	156.569	118.998	2.894	79.0375	**200.898**
80	1.490	19.160	113.684	108.609	1.479	22.381	**121.453**
90	1.185	4.593	57.015	**91.424**	1.181	4.372	**68.603**

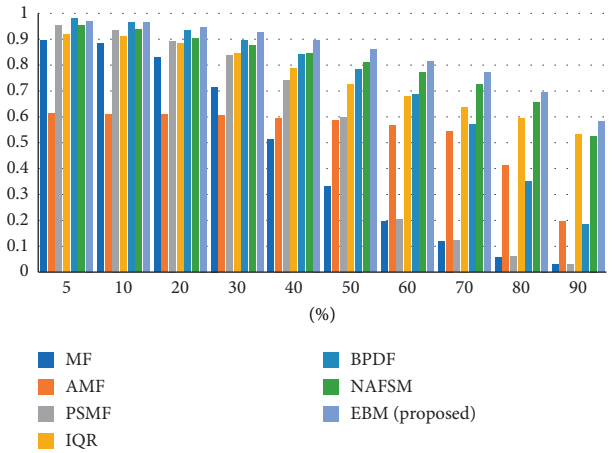

Figure 7: Comparison of SSIM for different denoising techniques (grey image-Lena).

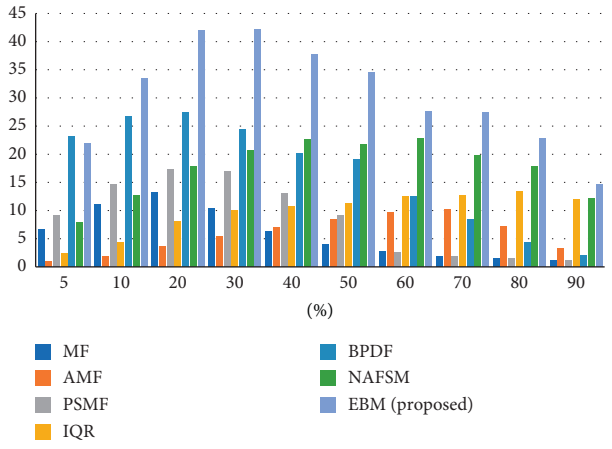

Figure 8: Comparison of IEF for different denoising techniques (grey image-Lena).

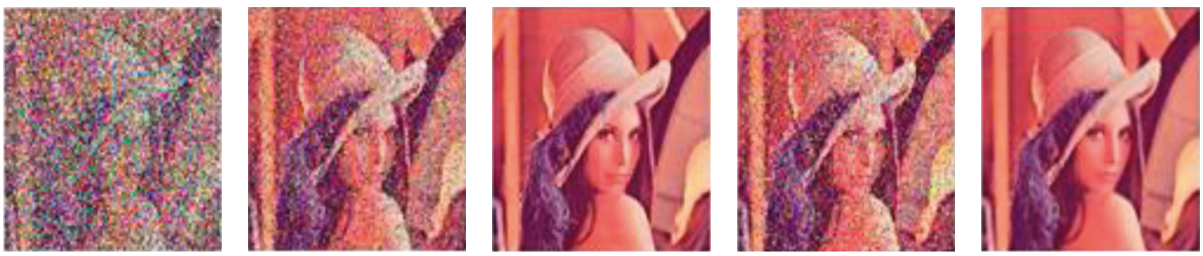

(a) (b) (c) (d) (e)

Figure 9: Continued.

(f) (g) (h)

Figure 9: Various method results with 30% noise density: (a) Image with noise density of 30%; (b) MF [8]; (c) AMF [9]; (d) IQR [15]; (e) AIQR [16]; (f) BPDF [18]; (g) NAFSM [13]; and (h) EBD.

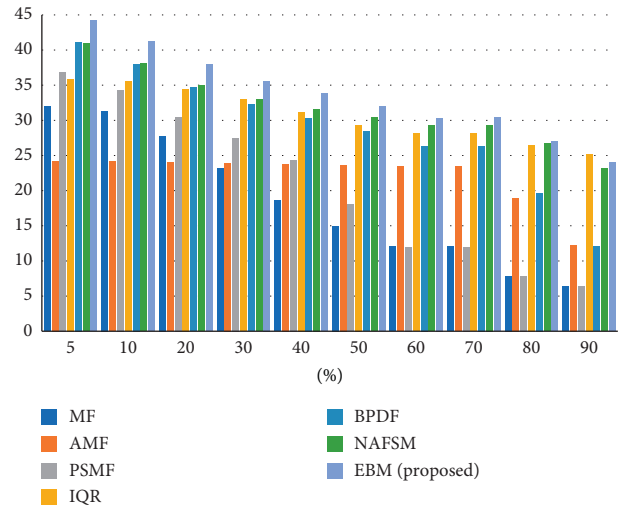

Figure 10: Comparison of PSNR for different denoising techniques (colour image-Lena).

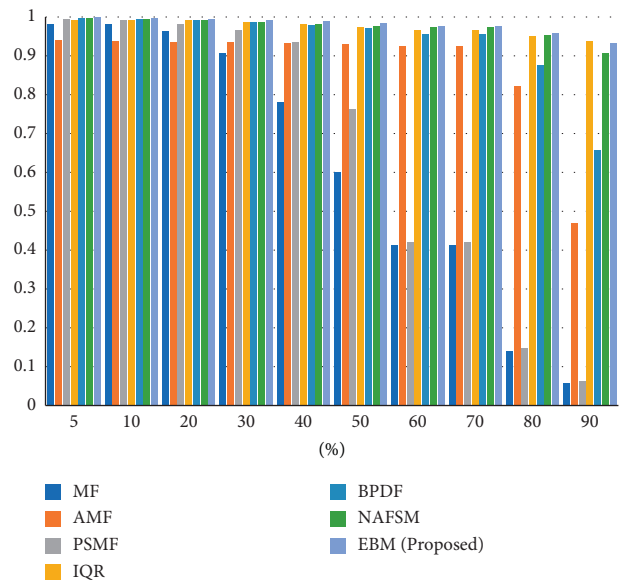

Figure 11: Comparison of SSIM for different algorithms (colour image-Lena).

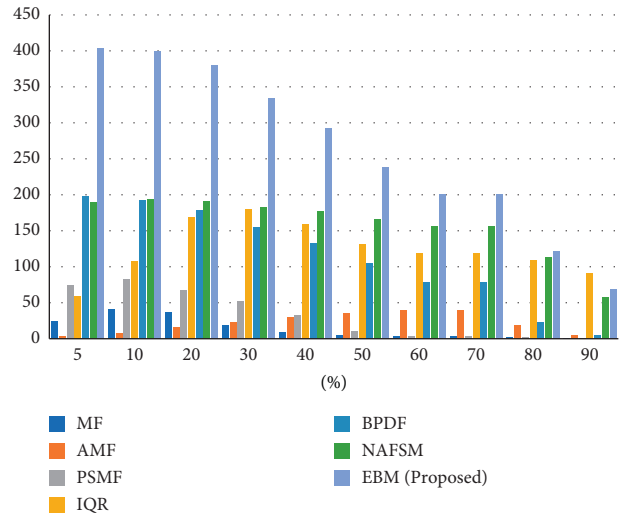

Figure 12: Comparison of IEF for different denoising algorithms (colour image-Lena).

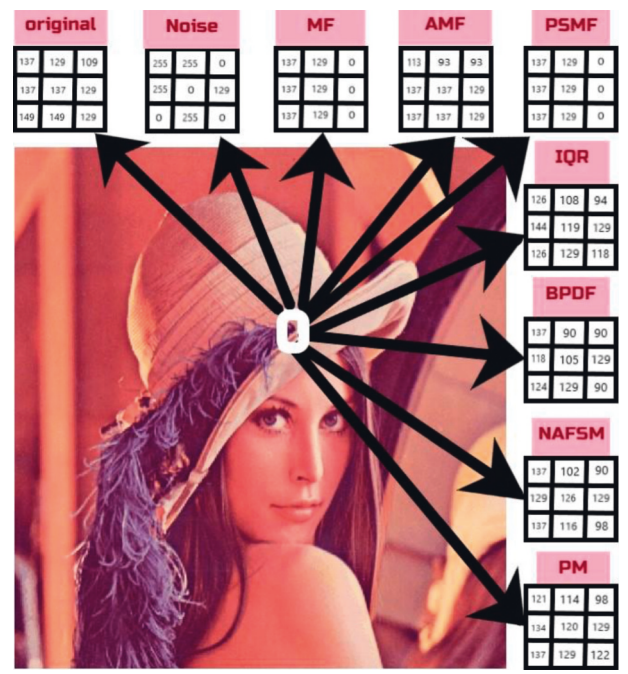

Figure 13: Comparison of different algorithms at pixel level [Lena-colour].

Now the same procedure was applied on colour images. The qualitative [visual] comparison results of the proposed method with the other standard methods are shown in Figure 9 for the Lena colour image with noise variances of 30% and 70%, respectively. The only difference between the greyscale and colour image is that colour image is processed with individual R, B, and G channels. The quantitative [tabular] analysis of the comparison is tabulated in Table 4 [PSNR], Table 5[SSIM], and Table 6 [IEF], respectively. It is observed that the proposed EBD method outperforms when the noise density is greater than 10%. The results of the proposed method are slightly less than the BPDF method when the noise variance is less than 5%. Figure 10 represents the comparison of PSNR metric on colour Lena image [29]. It is observed that the proposed denoising technique produces a high-quality image even when the noise levels are high. Similar graphical representations are shown in Figures 11 and 12 for the performance metric SSIM and IEF. Figure 13 depicts a crisp overview of various denoising techniques applied on the Lena image.

5. Conclusion

The proposed edge-based denoising method successfully discriminates edges while approximating the salt and pepper noises in the images. By considering the edge details with specific Sobel filters, the statistical quality also improved a lot. The performance of the algorithm was tested for different noise densities ranging from 5% to 90% on greyscale as well as on the colour images. The proposed EBD denoising technique has shown promising results when compared with the existing methods even for high noise levels. This was proved with the help of various noise metrics such as PSNR, SSIM, and IEF. It is concluded that the proposed algorithm is proved as an effective technique for the removal of salt and pepper noise in the grey as well as in the colour images, and also it is proved that it is computationally efficient method in identifying the edge from noise.

Data Availability

The data used to support the findings of this study are included within the article and further data or information can be obtained from the corresponding author upon request.

Conflicts of Interest

The authors declare that there are no conflicts of interest regarding the publication of this article.

References

[1] N. I. Crnojevic and V. Crnojevic, "Universal impulse noise filter based on genetic programming," *IEEE Transactions on Image Processing*, vol. 17, no. 7, pp. 1109–1120, 2008.

[2] M. S. R. Tanveer, K. M. R. Alam, M. A. Akash, and Y. Morimoto, "A technique to reconstruct wavelet-based watermark immune against salt & pepper noise," in *Proceedings of the 2019 4th International Conference on Electrical Information and Communication Technology (EICT)*, pp. 1–5, Khulna, Bangladesh, December 2019.

[3] T. Hong Ren Wu and H. R. Wu, "Adaptive impulse detection using center-weighted median filters," *IEEE Signal Processing Letters*, vol. 8, no. 1, pp. 1–3, Jan. 2001.

[4] S. Esakkirajan, T. Veerakumar, A. N. PremChand, and C. H. PremChand, "Removal of high density salt and pepper noise through modified decision based unsymmetric trimmed median filter," *IEEE Signal Processing Letters*, vol. 18, no. 5, pp. 287–290, May 2011.

[5] K. Aiswarya, V. Jayaraj, and D. Ebenezer, "A new and efficient algorithm for the removal of high density salt and pepper noise in images and videos," in *Proceedings of the 2nd Int. Conf. Computer Modeling and Simulation*, pp. 409–413, Hainan, China, January 2010.

[6] K. S. Ebenezer and D. Ebenezer, "A new fast and efficient decision-based algorithm for removal of high-density impulse noises," *IEEE Signal Processing Letters*, vol. 14, no. 3, pp. 189–192, Mar. 2007.

[7] X. L. Li, Y. T. Hu, X. B. Gao, D. C. Tao, and B. J. Ning, "A multi-frame image super-resolution method," *Signal Processing*, vol. 90, no. 2, pp. 405–414, 2010.

[8] P. Milanfar, "A tour of modern image filtering: new insights and methods, both practical and theoretical," *IEEE Signal Processing Magazine*, vol. 30, no. 1, pp. 106–128, 2013.

[9] C. S. S. Anupama, L. Natrayan, and E. Laxmi Lydia, "Deep learning with backtracking search optimization-based skin lesion diagnosis model," *Computers, Materials & Continua*, vol. 70, no. 1, pp. 1297–1313, 2021.

[10] S. S. Sundaram and N. Hari Basker, "Smart clothes with biosensors for ECG monitoring," *International Journal of Innovative Technology and Exploring Engineering*, vol. 8, no. 4, pp. 298–301, 2019.

[11] N. Iqbal, K. Ahmad, and W. Shahjehan, "High density impulse noise reduction by denoising neighbor pixels," in *Proceedings of the 13th International Conference on Emerging Technologies (ICET)*, pp. 1–5, Islamabad, Pakistan, December 2017.

[12] S. Esakkirajan, T. Veerakumar, A. N. Subramanyam, and C. H. PremChand, "Removal of high density salt and pepper noise through modified decision based unsymmetric trimmed median filter," *IEEE Signal Processing Letters*, vol. 18, no. No. 5, May 2011.

[13] H. Haddad and R. A. Haddad, "Adaptive median filters: new algorithms and results," *IEEE Transactions on Image Processing*, vol. 4, no. 4, pp. 499–502, April 1995.

[14] K. Rajagopalan and S. Angalaeswari, L. Natrayan, W. D. Mammo, "Combined economic emission dispatch of microgrid with the incorporation of renewable energy sources using improved mayfly optimization algorithm," *Computational Intelligence and Neuroscience*, vol. 2022, pp. 1–22, 2022.

[15] G. Kanimozhi, L. Natrayan, S. Angalaeswari, and P. Paramasivam, "An effective charger for plug-in hybrid electric vehicles (PHEV) with an enhanced PFC rectifier and ZVS-ZCS DC/DC high-frequency converter," *Journal of Advanced Transportation*, vol. 2022, Article ID 7840102, 14 pages, 2022.

[16] S. B. Sheik Fareed and S. S. Khader, "Fast adaptive and selective mean filter for the removal of high-density salt and pepper noise," *IET Image Processing*, vol. 12, no. 8, pp. 1378–1387, 2018.

[17] K. S. Srinivasan and D. Ebenezer, "A new fast and efficient decision-based algorithm for removal of high-density impulse

noises," *IEEE Signal Processing Letters*, vol. 14, no. 3, pp. 189–192, 2007.

[18] Y. H. Song, Y. S. Han, and J. S. Oh, S. Lee, "Edge preserving impulse noise reduction," *Journal of Imaging Science and Technology*, vol. 57, no. 6, pp. 60507–60511, 2013.

[19] K. K. V. Isa and N. A. Mat Isa, "Noise adaptive Fuzzy switching median filter for salt-and-pepper noise reduction," *IEEE Signal Processing Letters*, vol. 17, no. 3, pp. 281–284, March 2010.

[20] B. Roig and V. D. Estruch, "Localised rank-ordered differences vector filter for suppression of high-density impulse noise in colour images," *IET Image Processing*, vol. 10, no. 1, pp. 24–33, 2016.

[21] A. Mahapatra and S. S. Parida, K. Surana, P. Balamurugan, L. Natrayan, P. Paramasivam, "Energy auditing for efficient planning and implementation in commercial and residential buildings," *Advances in Civil Engineering*, vol. 2021, pp. 1–10, 2021.

[22] L. P. Natrayan and J. E. Sakthi shunmuga sundaram, "Analyzing the uterine physiological with MMG signals using SVM," *International journal of pharmaceutical research*, vol. 11, no. 2, pp. 165–170, 2019.

[23] S. Magesh, V. R. Niveditha, P. S. Rajakumar, and S. Radha RamMohan, "Pervasive computing in the context of COVID-19 prediction with AI-based algorithms," *International Journal of Pervasive Computing and Communications*, vol. 16, no. 5, pp. 477–487, 2020.

[24] K. D. Buch, "Decision based non-linear filtering using interquartile range estimator for Gaussian signals," in *Proceedings of the 2014 Annual IEEE India Conference (INDICON)*, pp. 1–5, Pune, India, December 2014.

[25] A.. Halder, "An adaptive non-linear statistical salt-and-pepper noise removal algorithm using interquartile range," *ELCVIA - Electronic Letters on Computer Vision and Image Analysis*, vol. 18, no. 1, pp. 76–91, 2019.

[26] P. Anil Kumar, K. Sateesh Kumar, and S. V. Padmaja Rani, "Hardware implementation of denoising using AIQR technique," *International journal of future generation communication and networking*, vol. 2, no. 20, pp. 1629–1641, 2020.

[27] P. Jain and V. Tyagi, "Spatial and frequency domain filters for restoration of noisy images," *IETE Journal of Education*, vol. 54, no. 2, pp. 108–116, 2013.

[28] L. Zhang, W. S. Dong, D. Zhang, and G. M. Shi, "Two-stage image denoising by principal component analysis with local pixel grouping," *Pattern Recognition*, vol. 43, no. 4, pp. 1531–1549, 2010.

[29] R. Guhathakurta, "Denoising of image: a wavelet based approach," in *Proceedings of the 2017 8th Annual Industrial Automation and Electromechanical Engineering Conference (IEMECON)*, pp. 194–197, Bangkok, Thailand, August 2017.

[30] B. Song, Z. Duan, Y. Gao, and T. Shao, "Adaptive BM3D algorithm for image denoising using coefficient of variation," in *Proceedings of the 22th International Conference on Information Fusion (FUSION)*, pp. 1–8, Ottawa, ON, Canada, July 2019.

[31] W. Zuo, L. Zhang, C. Song, and D. Zhang, "Texture enhanced image denoising via gradient histogram preservation," *Computer Vision and Pattern Recognition*, vol. 1, no. 2, p. 1203, 1210, June 2013.

[32] K. Bnou, S. Raghay, and A. Hakim, "A wavelet denoising approach based on unsupervised learning model," *EURASIP Journal on Applied Signal Processing*, vol. 2020, 2020.

[33] P. Asha, L. Natrayan, B. T. Geetha, J. R. Beulah, R. Sumathy, G. Varalakshmi, S. Neelakandan, IoT enabled environmental toxicology for air pollution monitoring using AI techniques," *Environmental Research*, vol. 205, Article ID 112574, 2022.

[34] K. Vaishali and V. R. Niveditha, "Guided container selection for data streaming through neural learning in cloud," *International Journal of System Assurance Engineering and Management*, vol. 16, pp. 1–7, 2021.

[35] D. Kumar Jain, S. K. Sah Tyagi, and S. Neelakandan, "Metaheuristic optimization-based resource allocation technique for cybertwin-driven 6G on IoE environment," *IEEE Transactions on Industrial Informatics*, vol. 18, no. 7, pp. 4884–4892, 2021.

[36] V. Patanavijit, "Performance analysis of denoising algorithm based on adaptive median filter under unsystematic intensity impulse and salt and pepper noise," in *Proceedings of the 2018 International Electrical Engineering Congress (iEECON)*, pp. 1–4, Krabi, Thailand, March 2018.

[37] S. Banerjee, D. Sarkar, D. Chowdhuri, and S. R. Chowdhuri, "High-density salt and pepper noise removal from colour images by introducing new enhanced filter," in *Proceedings of the 2021 International Conference on Intelligent Technologies (CONIT)*, pp. 1–6, Kartakata, India, April 2021.

[38] Y. Xing, J. Xu, J. Tan, D. Li, and W. Zha, "Deep CNN for removal of salt and pepper noise," *IET Image Processing*, vol. 13, no. 9, 2019.

[39] J. Brahmaiah Naik, G. Babu Kande, and C. Srinivasarao, "Logarithmic distance measure with improved vector pattern for content based image retrieval system," *The Imaging Science Journal, ISSN*, vol. 66, pp. 1368–2199, 2018.

[40] R. D. Limshuebchuey and M. Saejia, "Comparison of image denoising using traditional filter and deep learning methods," in *Proceedings of the 2020 17th International Conference on Electrical Engineering/Electronics, Computer, Telecommunications and Information Technology (ECTI-CON)*, pp. 193–196, Manhattan, NY, USA, June 2020.

[41] R. Singh, A. K. Dubey, and R. Kapoor, "Denoised autoencoder using DCNN transfer learning approach," in *Proceedings of the 2022 International Mobile and Embedded Technology Conference (MECON)*, pp. 446–449, Noida, India, March 2022.

[42] F. Wang, B. Yang, Y. Wang, and M. Wang, "Learning from noisy data: an unsupervised random denoising method for seismic data using model-based deep learning," *IEEE Transactions on Geoscience and Remote Sensing*, vol. 60, pp. 1–14, 2022.